

Published in final edited form as:

J Am Chem Soc. 2007 April 4; 129(13): 3955–3965. doi:10.1021/ja068059e.

Spectroscopic, Computational and Kinetic Studies of the μ_4 -Sulfide Bridged Tetranuclear Cu_2 Cluster in N_2O Reductase: pH Effect on the Edge Ligand and its Contribution to Reactivity

Somdatta Ghosh[†], Serge I. Gorelsky[†], Serena DeBeer George[§], Jeannine M. Chan[¶], Inês Cabrito[‡], David M. Dooley[¶], José J. G. Moura[‡], Isabel Moura[‡], and Edward I. Solomon^{*,†}

[†] Department of Chemistry, Stanford University, Stanford, California 94305, USA

[§] Stanford Synchrotron Radiation Laboratory, Stanford University, Stanford, CA 94309, USA

[¶] Department of Chemistry and Biochemistry, Montana State University, Bozeman, Montana 59717

[‡] Departamento de Química, CQFB, Faculdade de Ciências e Tecnologia, Universidade Nova de Lisboa, 2825-114 Caparica, Portugal

Abstract

A combination of spectroscopy and DFT calculations has been used to evaluate the pH effect at the Cu_Z site in *Pseudomonas nautica* (Pn) N_2OR and *Achromobacter cycloclastes* (Ac) N_2OR and its relevance to catalysis. Absorption, MCD, EPR with sulfur K-edge XAS spectra of the enzymes at high and low pH show minor changes. However, resonance Raman (rR) spectroscopy of Pn N_2OR at high pH shows that the 415 cm^{-1} Cu-S vibration (observed at low pH) shifts to higher frequency, loses intensity and obtains a 9 cm^{-1} ^{18}O shift, implying significant Cu-O character, demonstrating the presence of a OH^- ligand at the $\text{Cu}_I\text{Cu}_{IV}$ edge. From DFT calculations both protonation of the OH^- to H_2O or the $\mu_4\text{-S}^{2-}$ to $\mu_4\text{-SH}^-$ would produce large spectral changes which are not observed. Alternatively, DFT calculations including a lysine residue at an H-bonding distance from the $\text{Cu}_I\text{Cu}_{IV}$ edge ligand show that the position of the OH^- ligand depends on the protonation state of the lysine. This would change the coupling of the Cu-(OH) stretch with the Cu-S stretch, as observed in the rR spectrum. Thus the observed pH effect ($\text{pK}_a \sim 9.2$) likely reflects protonation equilibrium of the lysine residue which would both raise E^0 and provide a proton for lowering the barrier for the N-O cleavage and for reduction of the $[\text{Cu}_4\text{S}(\text{im})_7\text{OH}]^{2+}$ to the fully reduced 4Cu^I active form for turnover.

Keywords

absorption; MCD; EPR; rR; sulfur K-edge XAS; spectroscopy; DFT; TD-DFT calculations; kinetics

1. INTRODUCTION

N_2O is reduced by two electrons by the enzyme Nitrous oxide Reductase (N_2OR), in the last step of the bacterial denitrification cycle ($\text{N}_2\text{O} + 2\text{H}^+ + 2\text{e}^- \rightarrow \text{N}_2 + \text{H}_2\text{O}$).^{1,2} N_2OR s from various organisms have been isolated aerobically and anaerobically since 1982, however, only recently crystal structures of the enzyme (isolated under aerobic conditions) from three species, *Pseudomonas nautica* (Pn), *Paracoccus denitrificans* (Pd) and *Achromobacter cycloclastes*

(Ac), have been reported.^{3–7} N₂OR is a homodimeric enzyme, with each subunit containing an electron-transferring Cu_A site in the C terminal domain,^{8–11} and a catalytic Cu_Z site in the N terminal domain.¹² The Cu_A-Cu_Z distance within a monomer is ~40 Å, however the intermonomeric Cu_A-Cu_Z distance is ~10 Å,^{3,6,13} which is within the range for efficient electron transfer (ET) in a protein, thus suggesting the requirement for dimerization. The Cu_A site in N₂OR has a structure closely similar to that of the Cu_A site in the cytochrome oxidases.^{10,14–18} The Cu_Z site has a unique structural motif, consisting of a μ₄-sulfide bridged tetranuclear Cu cluster. There are seven histidine ligands coordinated to the Cu_Z site (two ligated each to Cu_{I,II,III} and one to Cu_{IV}), and a water derived ligand at the Cu_ICu_{IV} edge, which is the proposed substrate binding site (Figure 1A).^{3,6} The crystal structure of AcN₂OR shows the presence of two oxygen atoms (ascribed to a OH⁻ near Cu_I and a H₂O near Cu_{IV}) at the substrate binding site (Figure 1B).^{7,19}

N₂OR can be isolated in different redox states depending on whether it is isolated aerobically or anaerobically, and much spectroscopic data on the Cu_Z site have been published.^{5,12,20–24} The aerobically isolated form of N₂OR studied by crystallography has been spectroscopically characterized, and found to contain Cu_Z in the 1Cu^{II}/3Cu^I redox state with a total spin of ½.^{25,26} EPR data and density functional theory (DFT) calculations show that the unpaired electron is delocalized between two or more Cu atoms and the μ₄-sulfide, indicating that Cu_Z is a mixed-valence system.^{27–29}

Recently, we have shown that the Cu_Z cluster can be further reduced to the 4Cu^I form, on prolonged incubation with reduced methyl-viologen (MV).³⁰ This 4Cu^I form of the cluster has been determined to be the catalytically active form involved in N₂O reduction, which has been supported by Dooley and co-workers.³¹ DFT calculations indicate that the binding energy of N₂O to the 4Cu^I form of Cu_Z is higher than the resting 1Cu^{II}/3Cu^I redox form due to enhanced back-donation from the fully reduced Cu_Z cluster to the bent μ-1,3 bridged N₂O ligand. Recently, a detailed mechanism for N₂O reduction by the Cu_Z site has been developed using DFT calculations coupled to these data.³² These calculations suggest the possibility of a direct cleavage of the N-O bond in the Cu_Z-N₂O complex because of the low reaction barrier (18 kcal mol⁻¹), associated with stabilization of the transition state by a strong Cu_{IV}²⁺-O⁻ bond. The two copper atoms (Cu_I and Cu_{IV}) at the ligand binding site of the cluster play a crucial role in the reaction, as these Cu atoms are directly involved in N₂O binding, bending the ligand to a configuration (N-N-O angle ≈ 139°) that resembles the transition state, and contributing the 2 electrons needed for N₂O reduction. The other atoms of the Cu_Z cluster maintain the needed structural motif and make Cu_I and Cu_{IV} better electron donors to enhance the back-bonding required for N₂O activation.³²

Despite crystallographic, spectroscopic and computational studies on the Cu_Z, the nature of the Cu_ICu_{IV} edge ligand still remains ambiguous. In addition, the sulfide protonation of the cluster has not been experimentally evaluated. Past studies have defined the pH dependence of N₂OR activity, with an optimum activity in the range of pH 8–9.5 depending on the enzyme source.^{33–35} This could be attributed to a protonation equilibrium of the Cu_ICu_{IV} edge ligand, or a nearby residue involved in the rate determining step, or the μ₄-sulfide, or all three.

In this study we have used absorption, MCD, resonance Raman (rR), EPR and S K-edge spectroscopy to evaluate the effect of pH on the geometric and electronic structure of the Cu_Z clusters of PnN₂OR and AcN₂OR. A large change in the rR spectrum is observed with a pK_a of ~9.2. Spectroscopic studies have then been performed at a lower pH (6–7) and higher pH (10.5) to study the pure species present as an equal mixture at this pK_a.³⁶ We then use DFT calculations to analyze these results and elucidate the nature of the Cu_ICu_{IV} edge ligand. We have also computationally evaluated the various protonation states of the edge ligand, the μ₄-sulfide and a nearby lysine residue. The pH dependence of kinetics of the reduction of the

Cu₂ cluster has been determined to gain insight into the contributions of the protonation equilibrium towards reactivity.

2. EXPERIMENTAL METHODS

Materials

All reagents were of the highest grade commercially available and were used without further purification. PnN₂OR was aerobically isolated and purified in Tris buffer, as previously reported, and details of AcN₂OR expression and anaerobic purification will be reported elsewhere. The enzymes were exchanged to deuterated buffers at different pHs for spectroscopic and kinetic studies. Enzymatic activities and copper and sulfur contents were characterized as previously reported.^{4,5,30,31} Excess dithionite solution was added to reduce the Cu_A center to make it spectroscopically silent (inferred from EPR and absorption spectra), while the oxidation state of the Cu_Z site remained unchanged. Excess ascorbate solution with prolonged incubation was used to reduce the Cu_A site (inferred from EPR and absorption spectra) of the S K-edge XAS samples to avoid interfering sulfur signals from dithionite. Specific activities of the enzymes were measured by pre-incubating the enzyme with excess dithionite-reduced MV.^{30,31} Glassed samples for MCD experiments were prepared by adding 50% (v/v) buffer/glycerol-(OD)₃. Addition of glycerol had no effect on the CD/EPR spectra of the enzymes. Epsilon values (per dimer, containing two Cu_Z centers) reported have been estimated by EPR spin quantification. H₂¹⁸O (95–97% purity) was purchased from Cambridge Isotopes. Approximate concentrations of samples used for spectroscopy was 0.5 mM.

Spectroscopic Studies

Low-temperature absorption measurements were performed on a double beam spectrophotometer (Cary 500) using a liquid helium cryostat (Janis Research Super Vari-Temp). MCD data were collected on CD spectro-polarimeters (JASCO J810 with a S20 PM tube for the UV/Vis region, and J200 with an InSb detector for the near-IR region) with sample compartments modified to accommodate magnetocryostats (Oxford Instruments, SM4-7T). EPR spectra were obtained using a Bruker EMX spectrometer, ER 041 XG microwave bridge, and ER 4102ST cavity. All X band samples were run at 77 K in a liquid nitrogen finger dewar. A Cu standard (1.0 mM CuSO₄·5H₂O with 2 mM HCl and 2 M NaClO₄) was used for spin quantitation of the EPR spectra. Q band spectra were obtained at 77 K using an ER 051 QR microwave bridge, an ER 5106QT resonator, and an Oxford continuous flow CF935 cryostat. EPR spectra were baseline-corrected and simulated using XSophe (Bruker). For a given enzyme, X and Q band spectra were simultaneously fit in order to constrain the simulation parameters (g values were obtained from Q band and hyperfine constants from X band EPR). rR spectra were obtained using a series of lines from Kr⁺ (Coherent 190CK) and Ar⁺ (Coherent Sabre 25/7) ion lasers with incident power ranging from 10 to 50 mW in an ~135° backscattering configuration. Dye (Rhodamine 6G, Coherent 599) and Ti-Sapphire (Coherent 890) lasers were used for other spectral regions. Scattered light was dispersed through a triple monochromator (Spex 1877 CP, with 1200, 1800, and 2400 groove mm⁻¹ gratings) and detected with a back-illuminated CCD camera (Princeton Instruments ST-135). Samples contained in NMR tubes were immersed in a liquid nitrogen finger dewar. Raman peak intensities were referenced to the ice peak at ~230 cm⁻¹ for rR excitation profiles. Background spectra of charcoal in the same NMR tube were subtracted to remove the quartz scattering. Sulfur K-edge data were measured at the Stanford Synchrotron Radiation Laboratory under ring conditions of 3.0 GeV and 60–100 mA, using the 54-pole wiggler beam line 6-2 in high magnetic field mode of 10 kG with a Ni-coated harmonic rejection mirror and fully tuned Si (111) double crystal monochromator. Details of the optimization of this setup for low-energy studies have been described previously.³⁷ Protein samples were loaded in an inert atmosphere glove box and were immediately transferred to a helium purged sample space. Protein solutions

were loaded via syringe into a Pt-coated Al block sample holder with a 6.35- μm -thick polypropylene window. S K-edge measurements were made at $\sim 4^\circ\text{C}$. The data were measured as fluorescence excitation spectra utilizing an ionization chamber as a fluorescence detector. The energy was calibrated using the S K-edge spectrum of $\text{Na}_2\text{S}_2\text{O}_3 \cdot 5\text{H}_2\text{O}$, run at intervals between sample scans. The maximum of the first pre-edge feature in the spectrum was fixed at 2472.02 eV. A step size of 0.08 eV was used over the edge region. Data were averaged, and a smooth background was removed from all spectra by fitting a polynomial to the pre-edge region and subtracting this polynomial from the entire spectrum. Normalization of the data was accomplished by fitting a flattened polynomial or straight line to the post-edge region and normalizing the edge jump to 1.0 at 2490 eV.

Kinetic Studies

PnN_2OR (0.5mM) was buffer exchanged to different pHs and incubated with 500-fold excess of dithionite-reduced MV (250mM). Then the loss of one-hole Cu_Z EPR signal intensity was measured at different time intervals, normalized with respect to the spectrum of the dithionite-reduced sample collected at time = 0 min. The temperature for the kinetic measurements was 25°C .

Computational Details

The Cu_Z active site has been modeled as previously described (Figure S1 A,B). In order to probe the influence of the deprotonated/protonated lysine residue near the $\text{Cu}_I\text{Cu}_{IV}$ edge of the Cu_Z cluster, the molecular model in this work has been extended to include the lysine and phenylalanine residues (Figure S1 C,D). The total number of atoms in these extended simulations was 127–129 (64 heavy atoms). The C_β and C_γ atoms of the lysine residue and the carbon atoms of the phenylalanine residue were kept fixed during the geometry optimizations. The 6-311++G** basis set was used for the atoms of the active center (Cu_4SN_7), the edge ligands and the lysine $-\text{NH}_2/\text{NH}_3^+$ group and the 6-31G* basis set was used for the other atoms. The 6-311++G** basis set is necessary for accurate modeling of the Cu_Z cluster through the minimization of basis set superposition error effects both for energy and geometry-optimization results.

DFT calculations have been performed using the *Gaussian 03* program.³⁸ Spin-unrestricted DFT was employed to model the open-shell species. Optimized molecular geometries were calculated using the hybrid B3LYP exchange-correlation functional^{39,40,41} with tight SCF convergence criteria (10^{-8} a.u.). Wave function stability calculations were performed to confirm that the calculated wave functions corresponded to the ground state. Frequency calculations were performed to ensure that the stationary points were minima and to calculate vibrational spectra. Time-dependent DFT (TD-DFT) was used to calculate the energies and intensities of the 40 lowest-energy, spin-allowed electronic transitions. The calculated absorption energies and intensities were transformed with the *SWizard* program⁴² into simulated spectra as described before,⁴³ using Gaussians with half-widths ($\Delta_{1/2}$) of 3000 cm^{-1} .

Atomic charges and spin densities were calculated using the natural population analysis (NPA)⁴⁴ as implemented in *Gaussian 03*. The Mayer bond orders (BOs) were obtained to analyze covalent contributions to chemical bonding between the molecular fragments.^{45,46} The bond order contributions from α - and β -spin molecular orbitals (BO^α and BO^β , respectively) and atomic indices were calculated using the *AOMix-L* program⁴⁷ and used in the analysis of chemical bonding. These calculations (the bond order analysis and the calculation of atomic valence indices) were performed using TZVP⁴⁸ on the Cu_4S cluster, the edge ligands and the lysine $-\text{NH}_2/\text{NH}_3^+$ group, and 6-31G* on the other atoms.

3. RESULTS AND ANALYSIS

3.1. Spectroscopy

3.1.1. Absorption and MCD—The absorption and MCD spectra of the dithionite reduced (i.e. Cu_A reduced and Cu_Z in the $1\text{Cu}^{\text{II}}/3\text{Cu}^{\text{I}}$ redox state) samples of PnN_2OR (pH 10.5) and AcN_2OR at pH 6 and 10.5 are presented in Figure 2. Both the absorption and MCD spectra have intense S-Cu charge transfer (CT) bands at around 15600 cm^{-1} (640 nm), giving Cu_Z its characteristic blue color. The MCD spectrum of these enzymes also has an intense derivative shaped pseudo-A type signal in the S-Cu CT region. The absorption and MCD spectra of Cu_A -reduced PnN_2OR at pH 7 reported previously²⁶ (Figure S4A,B adapted from Ref. 26) have been simultaneously fit with thirteen bands (Table 1). Bands 1, 3, 4 and 8 were assigned as Cu d-d transitions, band 2 as inter-valence transition (IT), bands 5–7 the S-Cu CT transitions, and bands 9–13 the Histidine to Cu CT transitions. The orientations of the non-primed and primed axes systems in Table 1 are shown in Figure S2 and the details of these assignments are presented in Ref. 26.

The absorption and MCD spectra of the anaerobically isolated AcN_2OR reduced with dithionite (i.e. Cu_A reduced and Cu_Z in the $1\text{Cu}^{\text{II}}/3\text{Cu}^{\text{I}}$ form) at pH 6 are shown in Figure 2C, D. Simultaneous Gaussian fitting of the absorption and MCD spectra also give thirteen bands, which can be assigned in parallel with those of PnN_2OR . The spectra of PnN_2OR and AcN_2OR look very similar, but have some quantitative differences. In general, all the bands in AcN_2OR are blue shifted (Table 1). There is also intensity redistribution in the S-Cu CT bands in the absorption spectra of the two enzymes (Figures S4A and 2C), with band 5 being the most intense in AcN_2OR compared to band 6 in PnN_2OR . This is also reflected in the rR profiles (*vide infra*) and MCD spectra (Figures S4B and 2D), where the negative pseudo-A signal (band 5) is more intense in AcN_2OR than in PnN_2OR . Similar spectral differences can also be observed between the two enzymes at high pHs (Figure 2A, B, E, F). These reflect quantitative differences in S 3p contributions to the β -LUMO of the Cu_Z cluster in the two enzymes (see Discussion Section).

At high pH the absorption and MCD spectra of PnN_2OR (Figure 2 C, D) and AcN_2OR (Figure 2 E, F) show similar shapes and energy positions of the bands relative to the spectra at low pH, with minor perturbations in the higher energy Histidine to Cu CT region (band 9–13), indicating that the electronic structure of the Cu_Z cluster is not greatly perturbed on going from low to high pH for either enzyme.⁴⁹

3.1.2. EPR—Figure 3 shows the Q and X band EPR spectra of dithionite reduced (i.e. Cu_A reduced) samples of PnN_2OR (pH 10.5) and AcN_2OR (pH 6, 10.5). The g values of the enzymes have been extracted from Q band EPR data, which give the g_{\parallel} value and show that the Cu_Z cluster has an axial EPR signal with $g_{\parallel} > g_{\perp} > 2.003$ reflecting a $d_{x^2-y^2}$ ground state.

At pH 7, PnN_2OR has a g_{\parallel} value of 2.158 and g_{\perp} of 2.045 (Figure S5).²⁶ At pH 6, AcN_2OR has a g_{\parallel} value of 2.142 and g_{\perp} of 2.035 (Figure 3C, D, Table 2). Accurate g values obtained from Q band EPR spectra have then been correlated to the X band spectra. The g_{\parallel} values of both PnN_2OR and AcN_2OR map onto a hyperfine feature. Since the electron spin coupling to one Cu would lead to a g_{\parallel} positioned between the $M_s = +1/2$ and $-1/2$ hyperfine lines, at least two Cu atoms were required to account for the metal hyperfine splitting in the X band spectrum of both PnN_2OR and AcN_2OR . The results of the simulations (Table 2) show that PnN_2OR has A_{\parallel} of $61 \times 10^{-4}\text{ cm}^{-1}$ on one Cu and $23 \times 10^{-4}\text{ cm}^{-1}$ on the second Cu, indicating that the spin distribution on the two Cu atoms is in the ratio of 5:2, as published previously.²⁵ For AcN_2OR , A_{\parallel} values of $64 \times 10^{-4}\text{ cm}^{-1}$ and $41 \times 10^{-4}\text{ cm}^{-1}$ were obtained, indicating that the unpaired electron is distributed over two Cu atoms in the ratio of ~3:2. Simulation using three Cu atoms did not improve the goodness of fit.

The EPR spectra of both PnN₂OR and AcN₂OR do not change significantly on increasing the pH to 10.5 (Figure 3). The $g_{//}$ values remain almost the same while the $A_{//}$ values decrease by $4-8 \times 10^{-4} \text{ cm}^{-1}$ for the Cu atom with dominant $A_{//}$ contribution (Table 2). This implies that the spin density (SD) distribution is only slightly perturbed by changing the pH. This will be addressed in the Section 3.2.

3.1.3. Resonance Raman

(a) Vibrations: The rR spectra of PnN₂OR excited at 600 nm, and AcN₂OR excited at 620 nm at low and high pH in both ¹⁶O and isotope enriched ¹⁸O (95–97%) buffers are presented in Figure 4. PnN₂OR at pH 7 has three dominant peaks at 366, 386 and 415 cm⁻¹ (Figure 4A). Previous studies showed that these peaks shift to lower frequencies upon ³⁴S substitution.²⁰ Based on these isotope shifts, the vibrational frequencies and the excitation profiles, these rR features have been assigned as Cu-S stretching vibrations.²⁶ The ¹⁸O samples of PnN₂OR at the same pH showed no measurable shift in the energy positions of the three peaks, consistent with the assignment of these modes as having dominantly Cu-S character.

AcN₂OR at pH 7, also has three similar features at 366, 385 and 415 cm⁻¹ (Figure 4B) indicating a Cu₄S core similar to that of PnN₂OR. These also show no significant shift in the energy positions of the three peaks in ¹⁸O buffer.

The rR spectra of the two enzymes at high pH (excited at 600 nm and 620 nm for PnN₂OR and AcN₂OR respectively) are presented in Figure 4C,D. Importantly, in the case of PnN₂OR, the 415 cm⁻¹ band disappears, and another peak with lower intensity is present at 424 cm⁻¹ (Figure 4C). The rR profiles of the 415 cm⁻¹ (low pH) and 424 cm⁻¹ (high pH) vibrations are the same (*vide infra*), indicating that the corresponding vibrations are of similar origin. Thus, the 415 cm⁻¹ peak at low pH shifts to 424 cm⁻¹ at high pH. In the case of AcN₂OR, the peak at 415 cm⁻¹ has lost essentially all of its intensity at high pH, however no new rR vibration is observed (Figure 4D).

For PnN₂OR, ¹⁸O data obtained at high pH show a significant 9 cm⁻¹ shift of the 424cm⁻¹ peak to 415 cm⁻¹. The calculated ¹⁸O/¹⁶O shift for a mode with pure oxygen motion at this frequency is 24 cm⁻¹. Thus, the 9 cm⁻¹ ¹⁸O/¹⁶O shift indicates the presence of significant Cu-O character in the 424 cm⁻¹ vibrational mode at high pH. At low pH there is no ¹⁸O isotope shift, thus this mode is mainly Cu-S in nature. The loss of rR enhancement of the 415 cm⁻¹ mode in AcN₂OR at high pH (Figure 4D) may be a result of it having even higher Cu-O (relative to Cu-S) stretching character mixed in which would further decrease its resonance enhancement from a S-Cu CT transition.

(b) Profiles: The excitation profiles of the three dominant vibrations (366, 385/386 and 415 cm⁻¹), of both enzymes at low pH, overlaid with the absorption spectra with Gaussian fits (from absorption and MCD) are shown in Figure 5 A,B. As reported earlier, for PnN₂OR, the 415 cm⁻¹ mode mainly profiles band 7.²⁶ The 366 and 386 cm⁻¹ vibrations are mainly resonance enhanced by bands 5 and 6 of the absorption spectrum (Figure 5A). As mentioned in Section 3.1.1, the intensity pattern of the CT bands in the two enzymes is somewhat different. In the case of AcN₂OR, band 5 is the most intense, which is also reflected in the excitation profile (Figure 5B).

For AcN₂OR, the vibrations at 366 and 385 cm⁻¹ mainly profile absorption band 5 and weakly band 6 and the 415 cm⁻¹ vibration mainly profiles absorption bands 6 and 7. Since these vibrations are Cu-S stretches,²⁰ this supports the assignment of all three absorption bands as electronic transitions with substantial S-Cu CT character.

The rR profiles of the enzymes at high pH are presented in Figure 5C, D. For PnN₂OR, the rR profile at high pH is similar to that of low pH (Figure 5A,C), but with the 424 cm⁻¹ band (at high pH) having the same profile as the 415 cm⁻¹ at low pH. The intensity of the 424 cm⁻¹ vibration is much weaker than that of the 415 cm⁻¹ vibration at low pH. For AcN₂OR, at high pH, the vibrations at 366 and 385 cm⁻¹ mainly profile with absorption band 5 and 6. The 385 cm⁻¹ mode appears weakly enhanced by absorption band 7.

(c) pK_a: The pK_a of the one-hole form (1Cu^{II}/3Cu^I) of PnN₂OR and AcN₂OR were determined by plotting the relative rR intensities of the 415 cm⁻¹ peak (which decreased in intensity with increasing pH) and 424 cm⁻¹ peak (which increased in intensity with increasing pH) for PnN₂OR and the decreasing intensity of the 415 cm⁻¹ peak for AcN₂OR with increasing pH (it lacks the 424 cm⁻¹ peak at high pH) over a pH range of 7–11 (Figure 6). The pK_a for both enzymes was found to be ~9.2 (pK_a = 9.2±0.3 for PnN₂OR and 9.2 ± 0.4 for AcN₂OR). The pH-dependent rR data for both enzymes are provided in Figure S3.

3.1.4. S K-edges—Figure 7 shows a comparison of the normalized S K-edge spectra of AcN₂OR at pH 6.0 and 10. The spectra are essentially identical in both the rising edge region and the pre-edge region (expanded scale inset at 2469.2 eV). The energy of the pre-edge transition is very sensitive to the molecular environment of the μ₄-sulfide. The fact that the pre-edge does not change in intensity or energy between low and high pH indicates that protonation of the bridging sulfide does not occur at low pH. Protonation would stabilize the 1s orbital of the μ₄-sulfide and shift the pre-edge transition (S 1s→β-LUMO), to higher energy. The similar pre-edge intensity at both pHs indicates that the Cu-S covalency is unchanged. However, the S contribution to the β-spin LUMO cannot be quantitatively determined from the pre-edge intensity due to the errors associated with the large renormalization factor (32 S atoms contribute to the edge transition, while only one, μ₄-S of Cu_Z, contributes to the pre-edge feature)⁵⁰ and the incomplete Cu- and sulfide-loading in the protein.

To summarize the experimental data, from rR spectroscopy, we observe that the 415 cm⁻¹ vibration at low pH has dominant S character (from the ³⁴S isotope shift)²⁰ and no O character (lack of an ¹⁸O isotope shift). Upon increasing the pH, this vibration shifts to higher energy, its resonance enhancement is decreased and it now shows a 9 cm⁻¹ ¹⁸O isotope shift, indicating significant Cu-O stretching character. This strongly suggests the presence of a OH⁻ ligand in the Cu_ICu_{IV} edge of Cu_Z at high pH. From the absorption and MCD spectra of PnN₂OR and AcN₂OR at both high and low pHs, there is no significant change in the ligand field (LF). The EPR data at high and low pHs indicate that the SD distribution remains unperturbed over the pH transition. These results argue against a significant change in the edge ligand with pH. The S K-edge XAS data have identical pre-edge energies and intensities between the high and low pH forms suggesting that the μ₄-sulfide is not protonated in the one-hole form of the enzyme. Thus we conclude that the μ₄-sulfide and OH⁻ edge ligands remain preserved at low pH. We suggest that a conserved lysine residue that is at H-bonding distance to the edge ligand (~3–4Å) (Figure 1), is protonated with a pK_a of ~9.2, producing the observed pH effect. This is evaluated using DFT calculations below.

3.2. Computational

DFT calculations were used to obtain a detailed description of the 1Cu^{II}/3Cu^I state wave function (single unpaired electron, spin doublet) of the Cu_Z cluster of N₂OR in terms of how it is perturbed by different protonations. The geometric and electronic structures of the Cu_Z complexes with H₂O and OH⁻ (Figure 8) were evaluated to assess the influence of these ligands on the wave function and spectroscopic properties of the Cu_Z cluster. In the reported N₂OR structures, the Cu₄S core of the Cu_Z center has approximate C_s symmetry with the Cu_I-S-Cu_{II} angle (~160°) defining the mirror plane. The other Cu-S-Cu angles are close to 90°. The

experimental Cu-S distances are in the 2.15–2.35 Å range with the Cu_I-S bond being the longest.^{3–7} These structural features of the Cu_Z cluster are reproduced in the DFT calculations (Table S1).

In the [Cu₄S(im)₇(OH₂)]³⁺ species (Figures 8A and S1A), the water ligand is bound to only one copper atom, Cu_I.³² The weak Cu_Z-OH₂ bond with a distance of 2.23 Å and a bond order BO_{CuI-O} of 0.16 derives mostly from orbital interactions of the water ligand electron lone pair with the unoccupied Cu_I 4s orbital.³² As a result, the α- and β-spin components of the bond order BO_{CuI-O} are equal (0.08, Table S2). If the lysine residue near the Cu_ICu_{IV} edge is absent or non-charged (-NH₂ tail group), the OH⁻ ligand occupies a bridging position between the Cu_I and Cu_{IV} atoms (Figures 8B,D and S1B,D). This bridging binding mode has been recently reported for a Cu_Z complex with iodide in the X-ray structure of AcN₂OR.⁷ The bond orders BO_{CuI-O} and BO_{CuIV-O} are 0.56 and 0.38 respectively (Table S2), indicating a stronger covalent coupling between Cu_I and OH⁻. The α- and β-spin components of the bond orders for the Cu_Z-OH⁻ interaction (Table S2) indicate that the OH⁻ ligand binding involves charge donation to Cu 4s,4p orbitals and, to a lesser degree, the unoccupied β-spin Cu 3d orbital. However, as shown below, H-bonding between the OH⁻ ligand and the protonated lysine residue can influence the binding position of the OH⁻ ligand at the Cu_ICu_{IV} edge.

The ground state wave function and spin distribution in the Cu_Z cluster is influenced by the Cu_ICu_{IV} edge ligand (see below). In the Cu_Z cluster, Cu_I has the highest coordination number (CN) of 4 while the other Cu atoms have CNs of 2 and 3. In [Cu₄S(im)₇(OH)]²⁺, the valence indices⁴⁶ (Table S1) of the copper atoms are 2.20 (Cu_I), 1.96 (Cu_{II}), 1.90 (Cu_{III}) and 1.87 (Cu_{IV}). Since Cu_I has a stronger LF, as reflected by its atomic valence, it carries a higher charge and the unpaired electron is mostly-localized on this copper atom (31.5%, Table 3).

In [Cu₄S(im)₇(OH₂)]³⁺, the valence indices (Table S1) of the copper atoms are 1.96 (Cu_I), 2.12 (Cu_{II}), 2.26 (Cu_{III}) and 1.85 (Cu_{IV}). Since Cu_{IV} has the weakest LF, it carries only less than 4% SD, and Cu_I, Cu_{II} and Cu_{III} have SD of 16–19% each. Thus, the conversion from L=H₂O to L=OH⁻ should cause a noticeable change of the SD of the cluster (Table 3) which is not observed experimentally (Section 3.1). Such a change in the ground state wave function should also cause substantial change in the absorption spectrum of the Cu_Z cluster, especially in LF transitions as observed in TD-DFT-calculated absorption spectra of [Cu₄S(im)₇(OH₂)]³⁺ and [Cu₄S(im)₇(OH)]²⁺ (Figure 9). However, the absorption features of Cu_Z in the protein at low and high pH are very similar (Figures 2, S4). This observation argues that the protonation process with a pK_a of 9.2 is not associated with the transformation of the edge ligand between H₂O and OH⁻. Since the rR data provide strong evidence of OH⁻ binding to the Cu_Z cluster at high pH, the small changes in the absorption and EPR features of the Cu_Z cluster indicate that the OH⁻ ligand at the Cu_ICu_{IV} edge remains preserved at low pH.

Harmonic frequency calculations were performed to estimate vibrational frequencies of the Cu_Z species [Cu₄S(im)₇(OH)]²⁺ and evaluate ³⁴S and ¹⁸O isotope shifts of vibrational bands. The calculated data for the Cu_Z cluster are summarized in Figure 10. The vibrational modes of the Cu₄S cluster involve four Cu-S based stretching modes: two in-plane modes from Cu_I-S/Cu_{II}-S vibrations (both symmetric, assuming C_s symmetry for the Cu₄S cluster) and two out-of-plane modes, one symmetric combination of the Cu_{III}-S/Cu_{IV}-S stretches, and the other the antisymmetric combination of the Cu_{III}-S/Cu_{IV}-S stretches. Given the low symmetry of the Cu₄S cluster, this normal mode classification becomes somewhat approximate but still remains helpful. The Cu-S vibrational bands occur at 360–440 cm⁻¹ (Figure 4) and shift to lower frequencies upon ³⁴S isotope labeling.²⁰ However, they can kinematically couple with other metal-ligand vibrational bands such as Cu-imidazole and Cu-L (L=edge ligand) bands (Table S3) because the latter are also present in the low-frequency region of the vibrational spectrum and have force constants similar to those for the Cu-S stretching bands. The kinematic coupling

between the Cu-S and Cu-OH⁻ bands for the [Cu₄S(im)₇(OH)]²⁺ complex (Figure 10) is strong and the corresponding vibrations exhibit pronounced ³⁴S and ¹⁸O isotope shifts. This is consistent with the experimental data (Section 3.1) that indicate that at high pH the rR bands with mostly Cu-S character show a 9 cm⁻¹ ¹⁸O isotope shift for the 424 cm⁻¹ band of PnN₂OR. Note that if the OH⁻ is replaced by H₂O, the Cu-OH₂ frequency is greatly lowered and does not mix with the Cu-S core vibrations. (Table S4)

In the rR spectra of N₂ORs at low pH, three vibrational bands with significant Cu-S character have been identified at 366, 385/386 and 415 cm⁻¹ with ³⁴S isotope shifts of -2, -6 and -7 cm⁻¹, respectively,²⁰ and no detectable ¹⁸O isotope shifts. This indicates that, in going from high pH to low pH, the position of the OH⁻ ligand of the Cu_Z cluster is perturbed and the kinematic coupling between the Cu-S and Cu-OH⁻ bands is disrupted. Such a change can be caused by the strong non-covalent interaction between the OH⁻ ligand and the protonated lysine residue nearby. When the lysine residue is protonated, the proton of the -NH₃⁺ tail of the lysine functions as an H-bond donor to the OH⁻ ligand (the N_{lys}-O_{OH} distance is 2.90 Å) causing the ligand to move away from the Cu_{IV} atom ($\Delta d_{\text{CuIV-O}} = +1.25 \text{ \AA}$) and closer to the lysine -NH₃⁺ group (Table 3, Figures 8C and S1C). However, since the SD on the Cu_{IV} atom in [Cu₄S(im)₇(OH)]²⁺ is only 10% (Table 3), this change in the OH⁻ ligand position does not significantly perturb the ground state wave function. Consequently, the SD distribution in the Cu_Z cluster remains similar to that when the OH⁻ ligand occupied the bridging position at the Cu_ICu_{IV} edge (Table 3).

We also applied TD-DFT to probe the effect of possible protonation of the μ_4 -S ion on the absorption spectrum of the Cu_Z cluster at low pH (the [Cu₄SH(im)₇(OH₂)]⁴⁺ species, Figure 9, geometry optimized structure in Figure S6)⁵¹ as has been considered in Ref. 28. The calculated spectrum is very different from the spectra of the non-protonated Cu_Z species (Figure 9). The most pronounced spectral change is the disappearance of the strong CT bands near 15600 cm⁻¹ due to the stabilization of the μ_4 -S occupied orbitals and the significant blue shift of the corresponding S-Cu CT excitations. This is not observed experimentally. Combined with the fact that there is no change in the S K-edge spectrum of the protein at low pH (Section 3.1.4), this provides strong evidence that the small spectral changes observed upon pH variation in N₂ORs do not involve protonation of the μ_4 -sulfide of the Cu_Z cluster.

3.3. Kinetics

The rate of reduction of the resting one-hole (1Cu^{II}/3Cu^I) form of PnN₂OR to the fully reduced active form in the presence of 500-fold excess of reduced MV was measured at different pHs (Figure 11). The amount of one-hole Cu_Z was determined from the intensity of the Cu_Z EPR signal. The rate of reduction decreased with increase in pH. The rates have been simulated using a single exponential decay which gives low pH limit rate constant as 0.18 min⁻¹ (pH 7) and a high pH limit rate constant as 0.034 min⁻¹ (pH 10.5).⁵² Thus the rates of reduction differ by a factor of 5–6, on going from low to high pH, with a pK_a of ~9.0±0.2 (Figure 11 inset).

4. DISCUSSION

A combination of various spectroscopic techniques and DFT calculations has provided insight into the effect of pH on the geometric and electronic structure of the resting one-hole form of the Cu_Z clusters in PnN₂OR and AcN₂OR and the possible contribution of protonation to the rate determining step in turnover.

4.1. pH Effect

There is no observed change in the pre-edge energy and intensity of the S K-edge spectra of the one-hole form of AcN₂OR at low and high pHs, implying that there is no protonation of

the bridging μ_4 -sulfide at low pH. The TD-DFT-calculated spectrum of the μ_4 -sulfide form is in good agreement with the experimental absorption spectrum. However, it is significantly different from that of the spectrum of the μ_4 -SH⁻ form, [Cu₄SH(im)₇(OH₂)⁴⁺]. These results eliminate the possibility of a μ_4 -sulfide protonation of the Cu_Z cluster at low pH.

The rR data of PnN₂OR at high pH shows that the 415 cm⁻¹ Cu-S stretching vibration shifts to higher frequency, loses intensity and now shows a 9 cm⁻¹ ¹⁸O shift, while the 415 cm⁻¹ band in AcN₂OR loses all intensity at high pH. This implies significant Cu-O stretching character mixed into this high frequency mode, indicating the presence of a OH⁻ ligand bound at the edge. These experimental results at high pH are also supported by DFT calculations which show that the kinematic coupling between the Cu-S and Cu-OH⁻ modes for the [Cu₄S(im)₇(OH)]²⁺ complex is strong, resulting in pronounced ³⁴S and ¹⁸O isotope shifts of the vibrational frequencies. In contrast, the absorption, MCD and EPR spectra of the enzymes at both low and high pH do not detect significant perturbations of the ground state wave function. DFT calculated spin densities and the TD-DFT calculated absorption spectra of the enzyme with H₂O as the edge ligand are very different than the spectra of OH⁻ as the edge ligand, implying that the Cu_ICu_{IV} edge ligand remains OH⁻ in the low pH region.

The rR spectrum at low pH are significantly different from the high pH rR spectrum. The 415 cm⁻¹ vibration in the low pH form has dominant Cu-S character (from its ³⁴S isotope shift)²⁰ and no Cu-O character (lack of an ¹⁸O isotope shift), reflecting that the Cu-S vibration coupling to the OH⁻ ligand is perturbed in the pH transition. We propose that a highly conserved lysine residue, which is at the H-bonding distance from the edge ligand, is protonated at physiological pH (pK_a of ~9.2), which results in a change in the position of the OH⁻ ligand. DFT calculations, which include the lysine residue near the Cu_ICu_{IV} edge support this model, since the calculations yield a similar SD distribution for the Cu_Z cluster (as observed in absorption, MCD and EPR data), but different orientations of the OH⁻ ligand (which would lead to a different vibrational coupling in the rR spectrum) between protonated and deprotonated lysine forms (Figure 8C,D). Thus, the observed pH-dependent spectroscopic changes are most reasonably assigned to a protonation of the lysine residue near the Cu_ICu_{IV} edge of the Cu_Z cluster leading to its H-bonding to the OH⁻ ligand of Cu_Z (Scheme 1A).

4.2. Differences in the protein sites of PnN₂OR and AcN₂OR

There are some resolvable spectral differences between PnN₂OR and AcN₂OR. The $g_{//}$ and g_{\perp} values of AcN₂OR are smaller than PnN₂OR (Table 2) and the unpaired electron is more delocalized in Cu_Z of AcN₂OR (ratio of spin distribution on two Cu atoms is 3:2 compared to 5:2 for PnN₂OR from EPR spectroscopy). All the CT and LF bands are blue-shifted in AcN₂OR. Also band 5 in AcN₂OR gains intensity, as reflected in its absorption, MCD and rR profile data, compared to PnN₂OR. Interestingly, the IT band (band 2, Figure 2) in PnN₂OR is more intense than that in AcN₂OR. These differences between the two enzymes are consistent with the presence of an additional or more strongly bound edge ligand in AcN₂OR, as is reported in its crystal structure (Figure 1B).⁷ An additional/stronger ligand near Cu_{IV} would increase the SD on Cu_{IV} (due to the stronger LF), and will lead to enhanced S p_Z' (oriented along the Cu_{III}Cu_{IV} vector, Figure S2) mixing into the β -LUMO, which would be consistent with the enhanced intensity of band 5 (electron excitation from the occupied MO with the S p_Z' character to the β -LUMO, Table 1) in AcN₂OR. The IT transition reflects the coupling and electron delocalization between Cu_I and Cu_{II}, mediated by the bridging sulfide via the Cu_I-S-Cu_{II} σ - σ superexchange pathway.²⁶ A higher SD on Cu_{IV} would lead to a lower SD on Cu_{II} and thus a lower intensity of the IT band in AcN₂OR. An additional or more strongly bound edge ligand would also lead to an increased LF in AcN₂OR as is reflected from the blue-shifted transition energies and the lower EPR g value.

4.3. Relevance to Reactivity

Our past studies indicate that the one-hole ($1\text{Cu}^{\text{II}}/3\text{Cu}^{\text{I}}$) form of the Cu_Z cluster must be reduced to the 4Cu^{I} form to be catalytically active.^{30,31} The slow rate of reduction of the resting Cu_Z center (0.18 min^{-1} at pH 7) is much slower than the turnover rate ($\sim 10^3 \text{ sec}^{-1}$ for PnN_2OR at optimum pH of ~ 8). However, it is important to note that the reducing agent, MV, is not the physiological reductant of the enzyme. The experimental rate of reduction decreases with increase in pH, by a factor of 5–6, with a pK_a of 9.0 ± 0.2 (Figure 11), which is close to the pK_a we suggest to be associated with the lysine residue near the $\text{Cu}_I\text{Cu}_{IV}$ binding site. The protonated form of lysine can tune the redox potential of Cu_Z , making it more positive, and accelerate the reduction rate of the Cu_Z cluster.

In Ref. 32, we have calculated that the barrier (ΔG^\ddagger) for the direct cleavage of the N-O bond for $[\text{Cu}_4\text{S}(\text{im})_7\text{N}_2\text{O}]^{2+}$ is 18 kcal mol^{-1} .³² In the transition state, an electron is transferred from the Cu_Z cluster to N_2O , activating the oxygen atom of the N_2O ligand for protonation. The protonated lysine residue near the edge could further lower this activation barrier. Computationally, the barrier for N-O bond cleavage decreases to 9 kcal mol^{-1} with an acidic H-bond donor. The calculated free energy for the protonated cleavage product in the reaction mechanism generating $[\text{Cu}_4\text{S}(\text{im})_7(\text{OH})]^{3+}$ with 2Cu^{II} is $-28.8 \text{ kcal mol}^{-1}$ (Scheme 2).³² The reduction of the hydroxo species is energetically favorable, ($\Delta G = -29.6 \text{ kcal mol}^{-1}$ for an e^- from Cu_A) generating the corresponding one-hole hydroxo form $[\text{Cu}_4\text{S}(\text{im})_7(\text{OH})]^{2+}$. The proton coupled reduction of this form to the fully reduced form can be lowered by protonation of the lysine residue at low pH. The calculated free energy for this step is $-5.8 \text{ kcal mol}^{-1}$ (Scheme 2).

SUMMARY

We have determined that the $\text{Cu}_I\text{Cu}_{IV}$ edge ligand of the one-hole state of N_2OR is OH^- in both the low pH (active) and high pH (inactive) forms. Also the μ_4 -sulfide of Cu_Z remains deprotonated at low pH. The observed pH effect likely reflects a neighboring lysine residue, which can H-bond with the edge ligand at low pH. The protonated form of this lysine can increase the redox potential of Cu_Z and provide a proton to lower the barrier of the N-O bond cleavage and drive the reduction of the one-hole Cu_Z to the catalytically active fully-reduced form in the reaction cycle.

Supplementary Material

Refer to Web version on PubMed Central for supplementary material.

Acknowledgements

This research was supported by NIH Grant DK-31450 (E.I.S.), POCTI/BME/42265/2001 (I.M.), MCB-0347871 (D. M. D). S.I.G. is grateful to NSERC (Ottawa) for a postdoctoral fellowship. SSRL operations are funded by the Department of Energy, Office of Basic Energy Sciences. The Structural Molecular Biology program is supported by the National Institutes of Health, National Center for Research Resources, Biomedical Technology Program and by the Department of Energy, Office of Biological and Environmental Research.

References

1. Zumft WG. *Microbiol Mol Biol Rev* 1997;61:533. [PubMed: 9409151]
2. Zumft WG, Kroneck PMH. *Adv Inorg Biochem* 1996;11:1993.
3. Brown K, Tegoni M, Prudêncio M, Pereira AS, Besson S, Moura JJ, Moura I, Cambillau C. *Nat Struct Biol* 2000;7:191. [PubMed: 10700275]
4. Brown K, Djjinovic-Carugo K, Haltia T, Cabrito I, Saraste M, Moura JGG, Moura I, Tegoni M, Cambillau C. *J Biol Chem* 2000;275:41133. [PubMed: 11024061]

5. Prudencio M, Pereira AS, Tavares P, Besson S, Cabrito I, Brown K, Samyn B, Devreese B, Van Beeumen J, Rusnak F, Fauque G, Moura JJG, Tegoni M, Cambillau C, Moura I. *Biochem* 2000;39:3899. [PubMed: 10747777]
6. Haltia T, Brown K, Tegoni M, Cambillau C, Saraste M, Mattila K, Djinnovic-Carugo K. *Biochem J* 2003;369:77. [PubMed: 12356332]
7. Paraskevopoulos K, Antonyuk SV, Sawers RG, Eady RR, Hasnain SS. *J Mol Biol* 2006;362:55. [PubMed: 16904686]
8. Holm RH, Kennepohl P, Solomon EI. *Chem Rev* 1996;96:2239. [PubMed: 11848828]
9. Ferguson-Miller S, Babcock GT. *Chem Rev* 1996;96:2889. [PubMed: 11848844]
10. Kroneck PMH, Antholine WE, Riester J, Zumft WG. *FEBS Lett* 1989;248:212. [PubMed: 2542087]
11. Kroneck PMH, Antholine WA, Riester J, Zumft WG. *FEBS Lett* 1988;242:70. [PubMed: 2849565]
12. Farrar JA, Thomson AJ, Cheesman MR, Dooley DM, Zumft WG. *FEBS Lett* 1991;294:11. [PubMed: 1660405]
13. Rosenzweig AC. *Nat Struct Biol* 2000;7:169. [PubMed: 10700265]
14. Charnock JM, Dreusch A, Korner H, Neese F, Nelson J, Kannt A, Michel H, Garner CD, Kroneck PMH, Zumft WG. *Eur J Biochem* 2000;267:1368. [PubMed: 10691974]
15. Kelly M, Lappalainen P, Talbo G, Haltia T, van der Oost J, Saraste M. *J Biol Chem* 1993;268:16781. [PubMed: 8393874]
16. Scott RA, Zumft WG, Coyle CL, Dooley DM. *Proc Natl Acad Sci U S A* 1989;86:4082. [PubMed: 2542963]
17. Kroneck PMH, Antholine WE, Kastrau DHW, Buse G, Steffens GCM, Zumft WG. *FEBS Lett* 1990;268:274. [PubMed: 2166686]
18. Antholine WE, Kastrau DHW, Steffens GCM, Buse G, Zumft WG, Kroneck PMH. *Eur J Biochem* 1992;209:875. [PubMed: 1330560]
19. The X-ray structures of the enzymes were obtained using the crystals from the solutions of pH 7.6–8, which should correspond to the low pH forms of the Cu₂ species of the current study.
20. Alvarez ML, Ai JY, Zumft W, Sanders-Loehr J, Dooley DM. *J Am Chem Soc* 2001;123:576. [PubMed: 11456570]
21. Farrar JA, Zumft WG, Thomson AJ. *Proc Natl Acad Sci USA* 1998;95:9891. [PubMed: 9707571]
22. Rasmussen T, Berks BC, Sanders-Loehr J, Dooley DM, Zumft WG, Thomson AJ. *Biochem* 2000;39:12753. [PubMed: 11041839]
23. Dooley DM, McGuihl MA, Rosenzweig AC, Landin JA, Scott RA, Zumft WG, Devlin F, Stephens PJ. *Inorg Chem* 1991;30:3006.
24. Dooley DM, Moog RS, Zumft WG. *J Am Chem Soc* 1987;109:6730.
25. Chen P, DeBeer George S, Cabrito I, Antholine WE, Moura JJG, Moura I, Hedman B, Hodgson KO, Solomon EI. *J Am Chem Soc* 2002;124:744. [PubMed: 11817937]
26. Chen P, Cabrito I, Moura JJG, Moura I, Solomon EI. *J Am Chem Soc* 2002;124:10497. [PubMed: 12197752]
27. Chen P, Gorelsky SI, Ghosh S, Solomon EI. *Angew Chem, Intl Ed* 2004;43:4132.
28. Oganessian VS, Rasmussen T, Fairhurst S, Thomson AJ. *Dalton Trans* 2004;996
29. Rasmussen T, Berks BC, Butt JN, Thomson AJ. *Biochem J* 2002;807. [PubMed: 12049645]
30. Ghosh S, Gorelsky SI, Chen P, Cabrito I, Moura JJG, Moura I, Solomon EI. *J Am Chem Soc* 2003;125:15708. [PubMed: 14677937]
31. Chan JM, Bollinger JA, Grewell CL, Dooley DM. *J Am Chem Soc* 2004;126:3030. [PubMed: 15012115]
32. Gorelsky SI, Ghosh S, Solomon EI. *J Am Chem Soc* 2006;128:278. [PubMed: 16390158]
33. Coyle CL, Zumft WG, Kroneck PMH, Koerner H, Jakob W. *Eur J Biochem* 1985;153:459. [PubMed: 3000778]
34. Berks BC, Baratta D, Richardson DJ, Ferguson SJ. *Eur J Biochem* 1993;212:467. [PubMed: 8383047]
35. Yamaguchi K, Kawamura A, Ogawa H, Suzuki S. *J Biochem (Tokyo, Japan)* 2003;134:853.
36. Studies at a pH range of 8.5–9 (where enzyme activity is optimum), would lead to a 50:50 equilibrium mixture of the low and high pH forms of the Cu₂ species.

37. Hedman B, Frank P, Gheller SF, Roe AL, Newton WE, Hodgson KO. *J Am Chem Soc* 1988;110:3798.
38. Frisch, MJ., et al. Gaussian 03 Revision C02.
39. Perdew JP. *Phys Rev B* 1986;33:8822.
40. Becke AD. *Phys Rev A* 1988;38:3098. [PubMed: 9900728]
41. Becke AD. *J Chem Phys* 1993;98:5648.
42. Gorelsky, SI. SWizard. Department of Chemistry, York University; Toronto, ON: 1999. <http://www.sg-chem.net>
43. Gorelsky SI, Lever ABP. *J Organomet Chem* 2001;635:187.
44. Reed AE, Weinstock RB, Weinhold F. *J Chem Phys* 1985;83:735.
45. Gorelsky SI, Basumallick L, Vura-Weis J, Sarangi R, Hedman B, Hodgson KO, Fujisawa K, Solomon EI. *Inorg Chem* 2005;44:4947. [PubMed: 15998022]
46. Mayer I. *Chem Phys Lett* 1983;97:270.
47. Gorelsky, SI. AOMix Software Package. Department of Chemistry, York University; Toronto, ON: 1998. <http://www.sg-chem.net>
48. Schafer A, Huber C, Ahlrichs R. *J Chem Phys* 1994;100:5829.
49. In Ref. 26 a more significant change in MCD bands 4, 8, 9, 10 was observed with increase in pH. However this change appears to reflect a 10–15% contribution from oxidized Cu_A.
50. The edge in a S K-edge spectrum is a result of all S 1s→4p transitions, however the pre-edge feature is a S 1s→β-LUMO transition, and its intensity is proportional to the % orbital character of the μ₄-sulfide of Cu_Z in the mostly Cu 3d-based β-LUMO. Non coordinated S cannot contribute intensity to the pre-edge.
51. Protonation of the μ₄-S ion of Cu_Z is less favorable in energy relative to protonation of the OH⁻ edge ligand by ~108 kcal mol⁻¹ (ΔE_{el} at the B3LYP level, in vacuum).
52. The data at pH 9 have been simulated using a double exponential expression, taking into account the different rates of reduction of the low pH form and that of the high pH form.

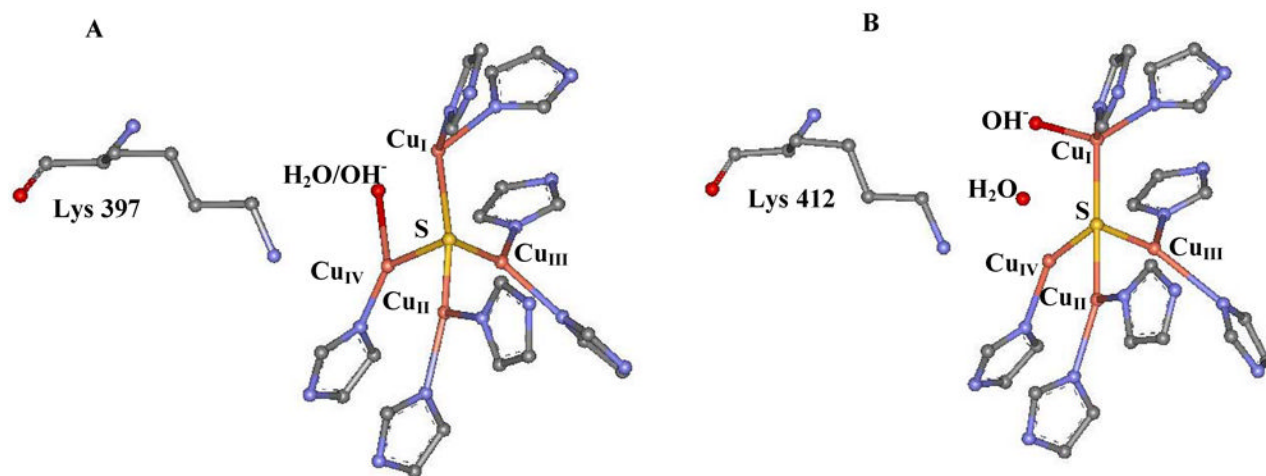


Figure 1. Crystal structures of A) PnN₂OR (PDB code 1QNI)³ and B) AcN₂OR (PDB code 2IWF)⁷ showing the Cu₂ cluster, the O atoms of the edge ligands, and the lysine residue near the cluster. The protonation states of the edge ligands cannot be assigned from the X-ray data.

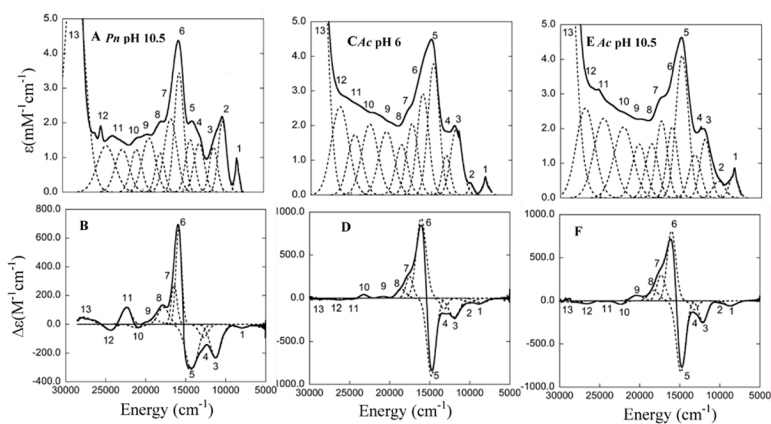


Figure 2. Optical spectra of dithionite-reduced Cu_2 : (A) PnN_2OR pH 10.5, 10K Absorption, (B) PnN_2OR pH 10.5, 5K, 7T MCD (C) AcN_2OR pH 6, 10K Absorption, (D) AcN_2OR pH 6, 5K, 7T MCD, (E) AcN_2OR pH 10.5, 10K Absorption, (F) AcN_2OR pH 10.5, 5K, 7T MCD.

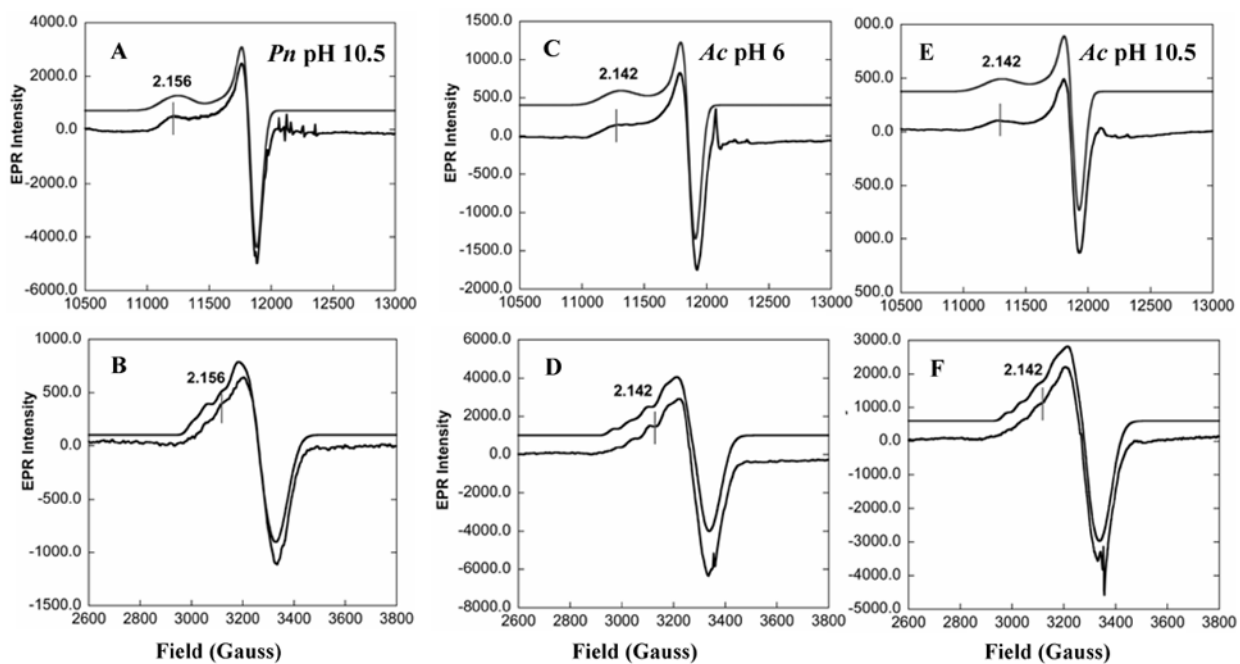


Figure 3.

Experimental (lower) and simulated (upper) EPR spectra of Cu_Z : (A) Q band, PnN_2OR , pH 10.5, (B) X band, PnN_2OR , pH 10.5, (C) Q band, AcN_2OR , pH 6, (D) X band, AcN_2OR , pH 6. (E) Q band, AcN_2OR , pH 10.5, (F) X band, AcN_2OR , pH 10.5. EPR spectra were collected at 77K, and 10mW power.

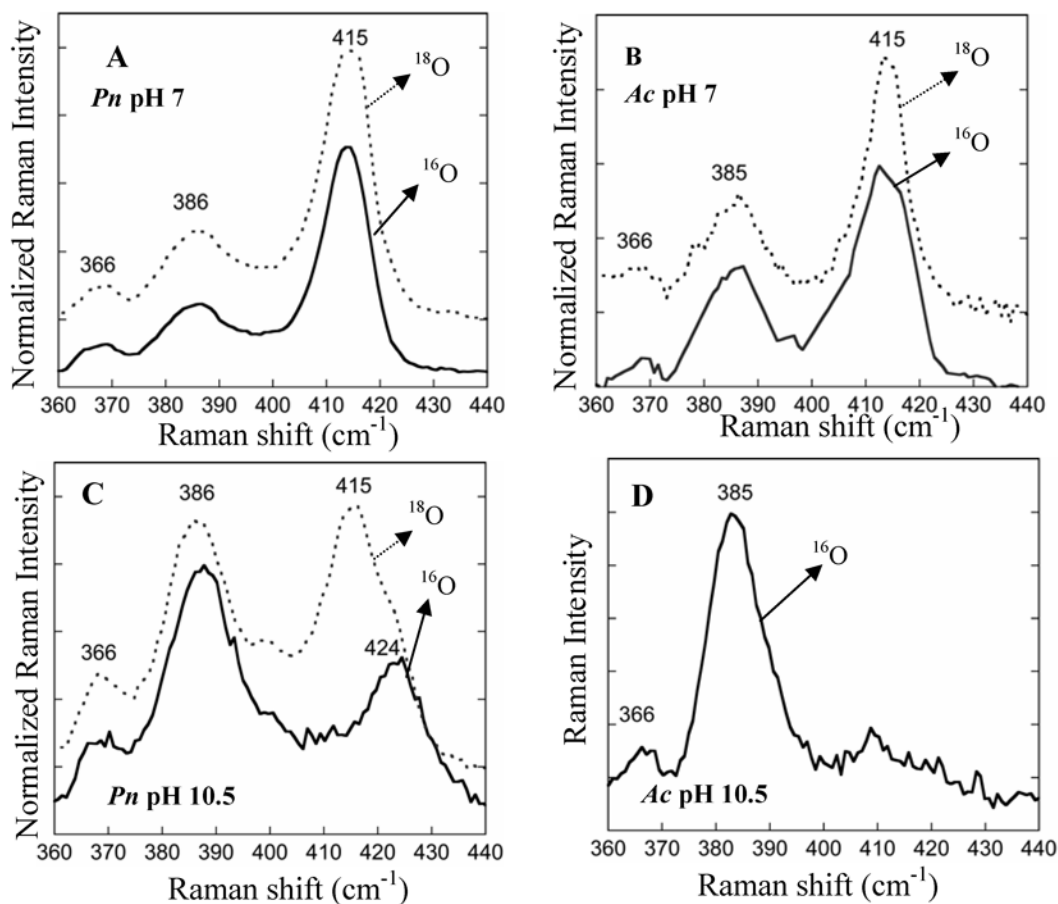


Figure 4.

Resonance Raman spectrum of Cu_2 from (A) PnN_2OR at pH 7, excited at 600nm. Ref. 26 showed PnN_2OR at pH 7 (^{16}O buffer), excited at 624.4nm (B) AcN_2OR at pH 7, excited at 620nm. (C) PnN_2OR at pH 10.5, excited at 600nm and (D) AcN_2OR at pH 10.5, excited at 620nm. Dotted lines (····) present data in ^{18}O , and bold lines (—) data in ^{16}O buffer. All data were collected at 77K. Y axes (A, B, C) are normalized to the ^{18}O independent 386 cm^{-1} (PnN_2OR) peak and the 385 cm^{-1} (AcN_2OR) peak. The ^{18}O data have been offset relative to the ^{16}O data. Note that data were not collected for ^{18}O samples of AcN_2OR at pH 10.5 since the 415 cm^{-1} or an equivalent mode was unobserved.

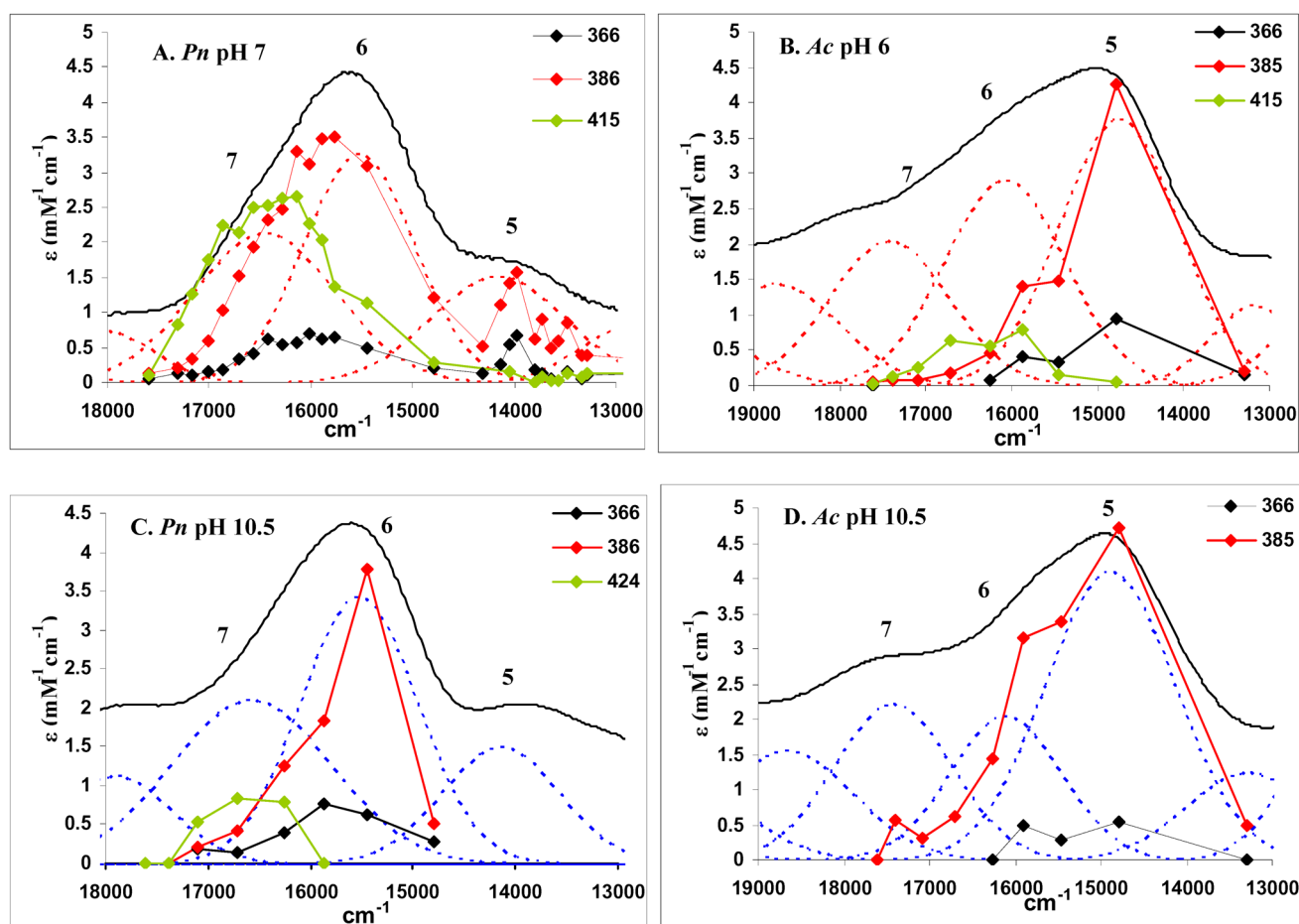


Figure 5. The Cu_2 resonance Raman excitation profiles overlaid on the Cu_2 absorption spectrum (solid line) with Gaussian fits (dotted lines) and band numbers : A) PnN_2OR , pH 7.0 (adapted from Ref. 26) B) AcN_2OR , pH 6.0, C) PnN_2OR , pH 10.5, D) AcN_2OR , pH 10.5.

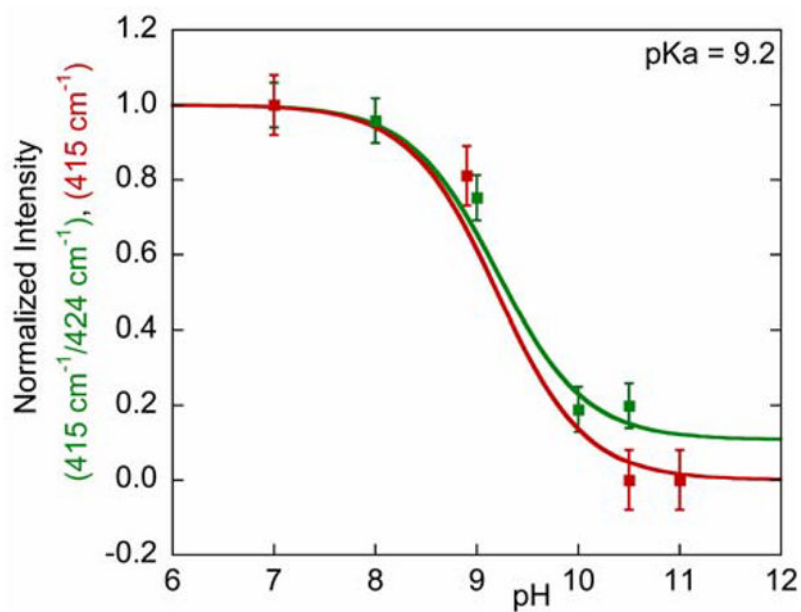


Figure 6. The pK_a plots for PnN₂OR determined from the relative intensities of the 415 to 424 cm^{-1} peaks excited at 600 nm (green) and AcN₂OR determined from the relative intensities of the 415 to 385 cm^{-1} peaks excited at 620 nm (red).

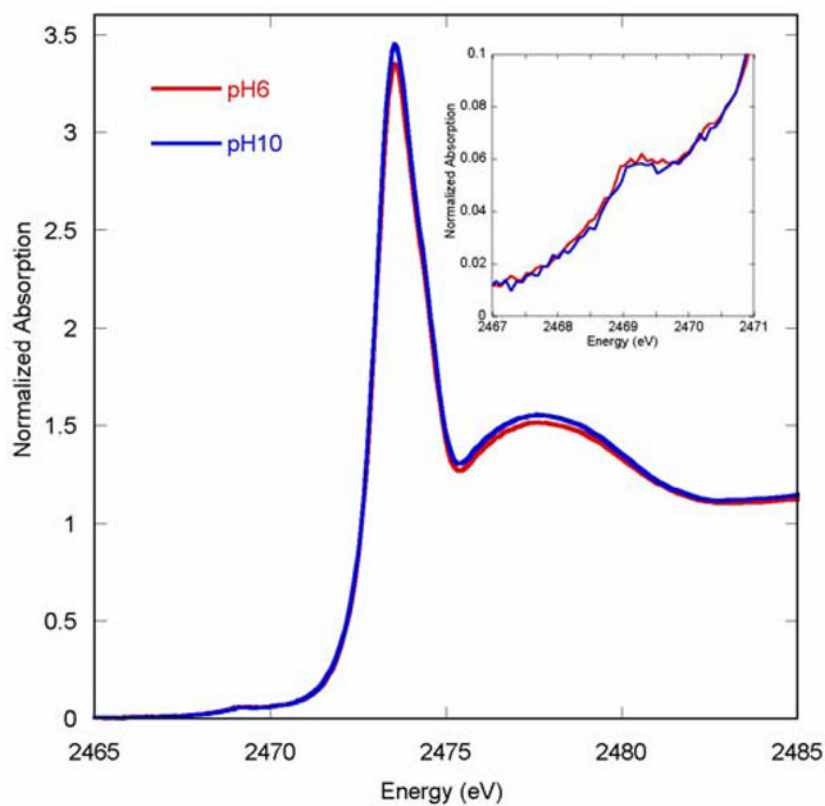


Figure 7. Normalized S K-edge spectra of AcN₂OR at pH 6 and 10, and an expansion of the pre-edge region (inset). Note the weak pre-edge feature at ~2470 eV corresponds to the presence of a small amount of oxidized Cu_A.

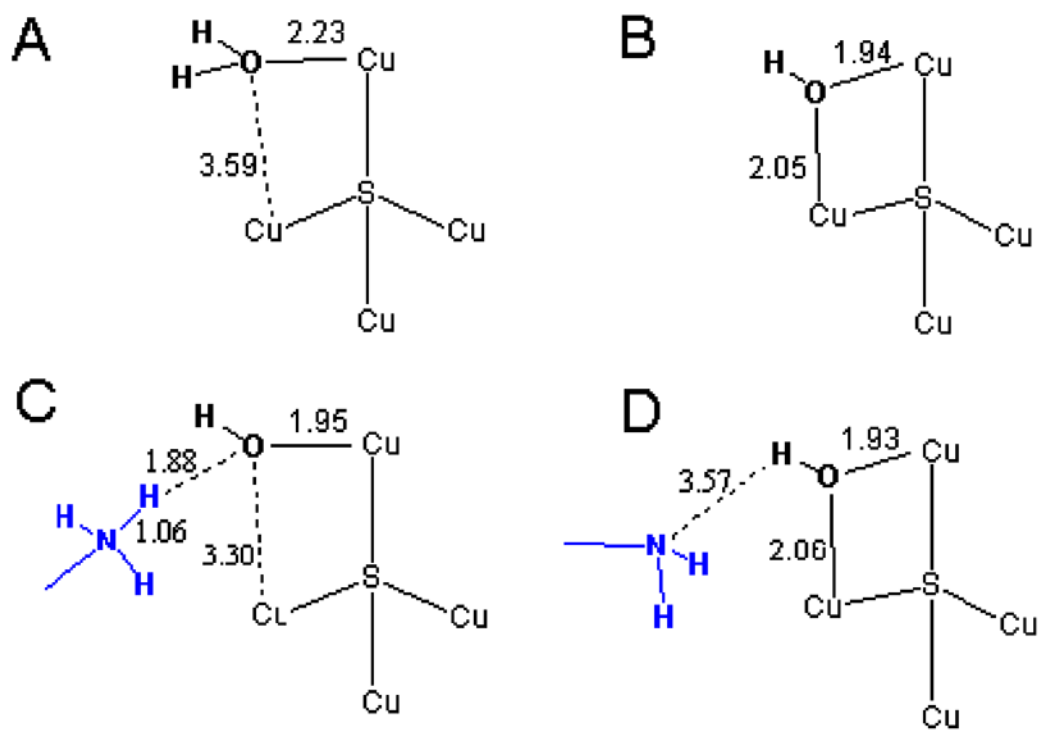


Figure 8.

The optimized structures of (A) $[\text{Cu}_4\text{S}(\text{im})_7(\text{OH}_2)]^{3+}$ and (B) $[\text{Cu}_4\text{S}(\text{im})_7(\text{OH})]^{2+}$ (adapted from Ref. 32) and (C) $[\text{Cu}_4\text{S}(\text{im})_7(\text{OH})]^{2+}$ with Lys and (D) $[\text{Cu}_4\text{S}(\text{im})_7(\text{OH})]^{2+}$ with LysH^+ . See Figure S1 for complete structures.

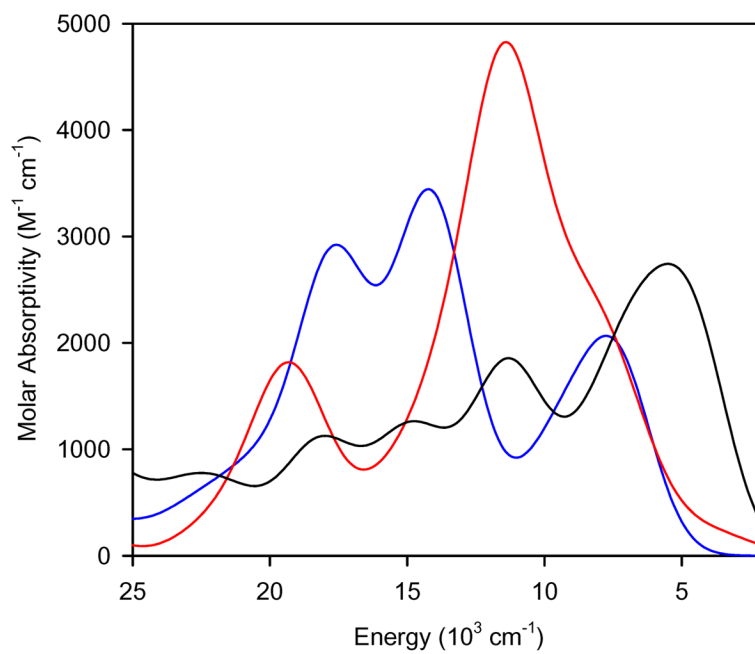


Figure 9. TD-DFT calculated absorption spectra of $[\text{Cu}_4\text{S}(\text{im})_7(\text{OH}_2)]^{3+}$ (blue line), $[\text{Cu}_4\text{S}(\text{im})_7(\text{OH})]^{2+}$ (red line) and $[\text{Cu}_4\text{SH}(\text{im})_7(\text{OH}_2)]^{4+}$ (black line).

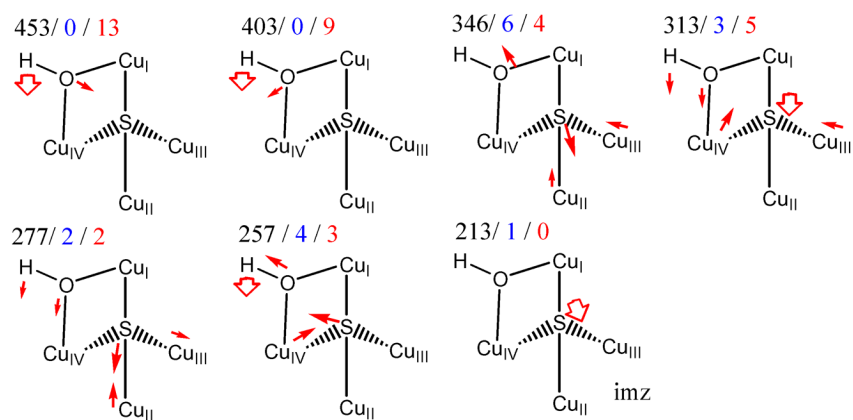


Figure 10.

Calculated Cu-S and Cu-OH normal modes of $[\text{Cu}_4\text{S}(\text{im})_7(\text{OH})]^{2+}$. The arrows indicate atomic displacements and band frequencies (cm^{-1}) and ^{34}S and ^{18}O isotope shifts (cm^{-1}) are shown in black, blue and red, respectively. The Cu-S and Cu-O bond length distortions for these bands are given in Table S3. The bands with significant imidazole displacement contributions are indicated by imz.

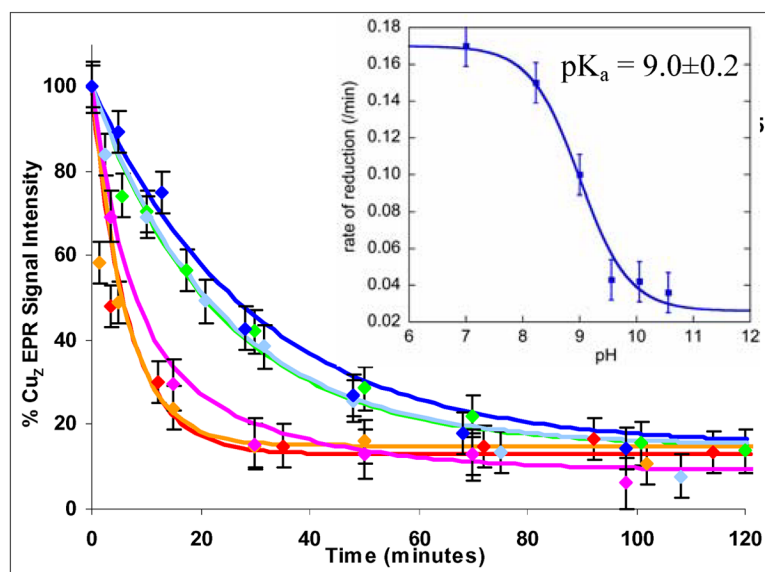
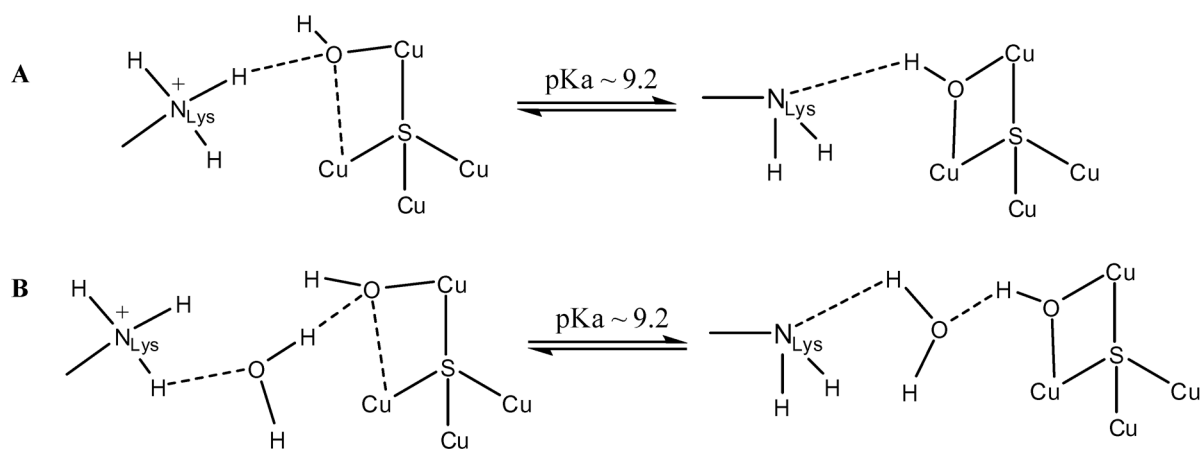
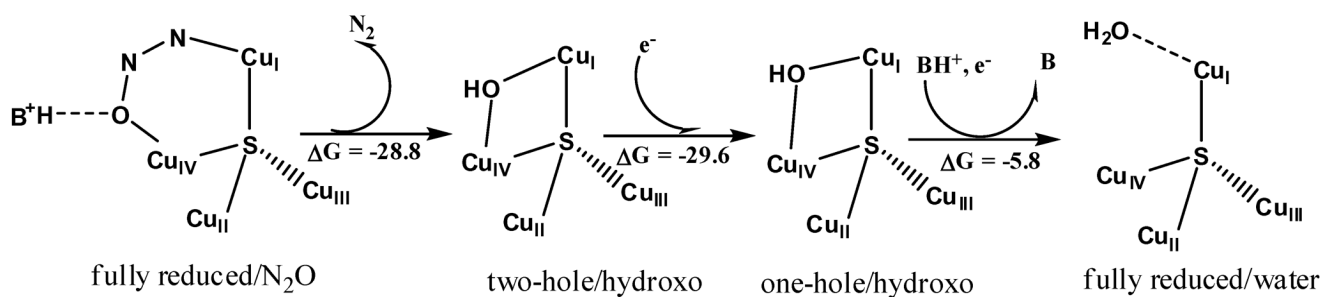


Figure 11. The rates of reduction of PnN_2OR at different pHs (red pH 7.0, orange pH 8.2, pink pH 9.0, green pH 9.5, light blue pH 10.0, blue pH 10.5). Inset: determination of $\text{pK}_a = 9.0 \pm 0.2$



Scheme 1.
pH effect in (A) PnN₂OR and (B) AcN₂OR.

**Scheme 2.**

Reaction mechanism for N_2O reduction by the Cu_2 cluster (energies in kcal mol^{-1}).

Gaussian resolved peak positions for absorption and MCD spectra of PnN_2OR and AcN_2OR at high and low pHs. The assignments are according to Ref. 26. The coordinate system is given in Figure S2.

Table 1

Band	assignment	$\nu_{\text{max}} (\text{cm}^{-1})$					
		$\text{PnN}_2\text{OR, pH 7}$		$\text{PnN}_2\text{OR, pH 10.5}$		$\text{AcN}_2\text{OR, pH 10.5}$	
1	$\text{Cu } d_{z^2}$	8015	8100	8400	8500		
2	Π	10000	10100	10100	10200		
3	$\text{Cu } d_{xz}$	11140	11250	11950	12050		
4	$\text{Cu } d_{yz}$	12900	12900	13200	13225		
5	$S P_x'$	14300	14200	14768	14900		
6	$S P_x'$	15675	15700	16070	16070		
7	$S P_y'$	16520	16500	17480	17380		
8	$\text{Cu } d_{xy}$	17980	17820	18600	18450		
9	Π_1	19775	19136	20700	20300		
10	Π_1	20985	20980	22950	22261		
11	Π_1	22270	22500	24600	24600		
12	Π_1	24030	24500	26300	26700		
13	Π_2	28055	28150	28600	29600		

Table 2

EPR parameters of AcN₂OR and PnN₂OR at low and high pHs, simulated with spin densities distributed on two Cu atoms.

Enzyme, pH	g	g _⊥	A	A _⊥ (×10 ⁻⁴ cm ⁻¹)	A ²	A _⊥ ²
PnN ₂ OR, 7.0	2.158	2.045	61	25	23	20
PnN ₂ OR, 10.5	2.156	2.042	57	24	24	20
AcN ₂ OR, 6.0	2.142	2.035	64	22	41	20
AcN ₂ OR, 10.5	2.142	2.032	56	22	37	20

Table 3

Atomic spin densities (NPA) of the Cu₂ cluster for the complexes with the edge ligand L and the Cu-O_L distances.

Species	NPA atomic spin density (%)				Cu-O _L distances (Å)		
	Cu _I	Cu _{II}	Cu _{III}	Cu _{IV}	S	Cu _I -O	Cu _{IV} -O
[Cu ₂ S(im) ₇ (OH ₂) ³⁺ ·a	17.1	15.9	18.8	3.7	31.1	2.23	3.39
[Cu ₂ S(im) ₇ (OH)] ²⁺ ·a	31.5	5.9	4.1	10.1	29.9	1.94	2.05
[Cu ₂ S(im) ₇ (OH)] ²⁺ ...LysH ⁺	44.9	6.3	3.2	3.6	21.3	1.95	3.30
[Cu ₂ S(im) ₇ (OH)] ²⁺ ...Lys	33.6	6.4	3.4	9.2	30.4	1.93	2.05

^a) adapted from Ref. 32.